Authors: I. Ayyubov, C. Berghian-Grosan, E. Dodony, Z. Pászti, I. Borbáth, A. Szegedi, A. Vulcu, A. Tompos & E. Tálas

Title: Structure - Catalytic Behavior Relationships in TiO_2-Carbon Composite Supported Pt Electrocatalysts: A Case Study.

Journal: Analytical Letters

DOI:10.1080/00032719.2024.2351589

Published online: 15 May 2024

Document type: Article

ISSN: 00032719

Structure - catalytic behavior relationships in TiO_2-carbon composite supported Pt electrocatalysts: a case study

Ilgar Ayyubov[1,2], Camelia Berghian-Grosan[3], Erzsébet Dodony[4], Zoltán Pászti[1], Irina Borbáth[1], Ágnes Szegedi[1], Adriana Vulcu[3*], András Tompos[1], Emília Tálas[1*]

[1]*HUN-REN Research Centre for Natural Sciences, Institute of Materials and Environmental Chemistry, Magyar tudósok körútja 2, H-1117 Budapest, Hungary*

[2]*Budapest University of Technology and Economics, Faculty of Chemical Technology and Biotechnology, Department of Physical Chemistry and Materials Science, Műegyetem rkp. 3, H-1111 Budapest, Hungary*

[3]*National National Institute for Research and Development of Isotopic and Molecular Technologies, 67-103 Donat Street, 400293 Cluj-Napoca, Romania*

[4]*HUN-REN Centre for Energy Research, Institute for Technical Physics and Materials Science Konkoly-Thege M. út 29-33, H-1121 Budapest, Hungary*

Abstract

Composite type of supports made of TiO_2 and carbonaceous materials provide higher stability for the Pt electrocatalysts under the working conditions of polymer electrolyte membrane fuel cells than the traditional carbon supports. We have demonstrated in our previous works that composites describing with general formula of 75 wt.% $Ti_{(1-x)}Mo_x$-25 wt.% C (x=0-0.2; C= traditional Black Pearls (BP) carbon) were promising supports which provided increased stability for the Pt electrocatalysts. In this work, the effect of nitrogen doping of the carbonaceous component of the composite was explored. 75 wt.% TiO_2-25 wt.% carbon composite supports were prepared using graphite oxide (GO), N-doped GO and N-doped multilayer graphene. Electrocatalysts were made by loading the supports with 20 wt.% Pt. The systems were compared based on their physicochemical properties determined by low temperature nitrogen adsorption, X-ray powder diffraction (XRD), Transmission Electron Microscopy (TEM), X-ray photoelectron spectroscopy (XPS) and conductivity measurements. The activity of the catalysts was investigated by conventional methods in 3-electrode electrochemical cell. The results of various characterization methods contributed to the understanding of the difference in the electrochemical behavior of N-free and N-containing catalyst samples. While GO provided favorable properties for this composite supported catalyst, its N-doping strongly influenced the growth of TiO_2, forming an almost continuous coating of small TiO_2 crystals. This quasi-insulating TiO_2 layer between the Pt catalytic sites and the conductive part of the composite resulted in poor electrochemical activity. Mixing the sample with carbon, however, improved its conductivity, which resulted in significant increase in the oxygen reduction reaction activity.

Keywords

graphite oxide, N-doped graphite oxide, N-doped multilayer graphene, composite support, electrocatalyst

*Corresponding authors, Tel.: +40264584037, email: avulcu@itim-cj.ro, address: 67-103 Donat St. Cluj-Napoca, Romania (Adriana Vulcu); Tel.: +36 1 382 6916, email: talas.emilia@ttk.hu, address: H-1519 Budapest, P.O.Box 286, Hungary (Emília Tálas)

Introduction

Since the widely used carbon supported platinum catalyst (Pt/C) suffers from electrocorrosion, development of active and stable electrocatalysts is one of the biggest challenges in the research of polymer electrolyte membrane fuel cells (PEMFCs) (Meier 2012, 2014). Due to the fact that the corrosion of carbon contributes significantly to the degradation processes (Zhao, J. 2021), composites made of inorganic - and carbonaceous material can provide higher stability for the supported Pt than the commercial carbon (Ayyubov 2021a; Borbáth 2021a; Zana 2014). Although several possibilities have been described in the literature to increase the stability by modified metal oxide electrodes (Karabiberoğlu 2019) and great number of various inorganic compounds has been tested as electrocatalyst supports (Özdokur 2022), TiO_2 seems to be a suitable inorganic component because of its stability during the polarization cycles in the acidic media of PEMFCs. Moreover, strong metal-support interaction (SMSI) which can appear between the Pt and the TiO_2 part of the composite can contribute to the further stabilisation of the supported Pt (Cao 2020; Hsieh 2017; Jiménez-Morales 2018). The carbonaceous part plays decisive role in the usability of the TiO_2-C composite as a support since high electrical conductivity and high specific surface area (SSA) are among the main requirements of a well-functioning electrocatalyst (Zhang, Z. 2014). In case of TiO_2, these parameters have limitations, while the carbonaceous component of the composite (i) can contribute to achieve the appropriate conductivity, (ii) can behave as template to obtain high specific SSA especially in case of composites prepared by sol-gel method (Borbáth 2021a). We have demonstrated in our previous works that composites described with general formula of 75 wt.% $Ti_{(1-x)}Mo_x$-25 wt.% C (x=0-0.2; C= traditional Black Pearls (BP) carbon) were promising supports which provided increased stability for the Pt electrocatalysts (Ayyubov 2021a; Vass 2019; Yazici 2021).

Non-traditional carbons, such as graphene nanosheets (GNS) were also able to increase the stability of supported Pt nanoparticles (Antolini 2012). Graphite oxide (GO) is very often used as starting material for GNS because it is relatively cheap, available in great amount and is relatively easy to handle due to its hydrophilic character (Lerf 2006). Its thermal, chemical and mechanical delamination followed by reduction results in reduced graphene oxide (rGO) which is frequently mentioned as “graphene” support (Zhang, N. 2015). However, layers of GNS tend to stacking which decreases the utilization of Pt supported by them, therefore spacer materials, such as inorganic materials (Mu 2016), conductive carbon (Park 2011; Neaţu 2021

and the references cited herein), carbon nanotubes (CNT) (Yun 2011) etc. are frequently built in between the layers.

Another often studied group of the carbonaceous materials is the nitrogen-doped carbon (N-C) (Wang, H. 2012 and the references cited herein). Various types of N-C materials such as N-doped CNT, N-doped graphene, N-doped carbon aerogels (Nagy 2016, 2018), N-doped ordered mesoporous carbon, (Wong 2013 and the references cited herein) N-doped GO (Ayyubov 2022) etc. have been tested in ORR as Pt free catalysts. In particular, a lot of work deals with N-doped graphene although its large-scale production was thought to be problematic (Wang, H. 2012). Recently, a mechanochemical method was identified as a relatively easy and sustainable way for production of N-doped graphene-like materials (Ayyubov 2022; Carrillo-Rodríguez 2017; Dan 2021; Xing 2013). Bonding configurations for nitrogen atoms in N-graphene were described as pyridinic $^{+}$N-O^{-}, quaternary N, pyrrolic N and pyridinic N (Wang, H. 2012 and the references cited herein). The spin density and charge distribution of carbon atoms is influenced by the N dopant in its close vicinity therefore N-graphene shows different properties compared to the pristine graphene (Wang, H. 2012 and the references cited herein). Due to the stronger interactions, N-C materials as catalyst supports were found to provide higher stability of the supported noble metal nanoparticles compared to the non-doped carbons (González-Hernández 2020; Imran Jafri 2010; Wong 2013 and the references cited herein). Although TiO_2-(N-C) composites have been tested in the field of photocatalysis (Gopalakrishnan 2011; Ida 2019; Lin 2017; Zheng 2020), photo assisted degradation (Zhao, Y. 2020), analytical chemistry (Patil 2021) and sensor technology (Ni 2018; Yan 2016), less information is available on their electrocatalytic behavior. Recently, these types of composites has been successfully applied as non-noble bifunctional electrocatalysts for ORR and oxygen evolution (OER) reactions in alkali media (Luque-Centeno 2021), however, to the best of our knowledge TiO_2-(N-C) composites has never been tested as support of Pt catalyst for PEMFCs.

The aim of this work was to prepare 75 wt.% TiO_2-25 wt.% C composite supports by use of GO as a non-traditional carbon and various N-containing carbon materials such as N-doped GO (NGO) and N-doped multilayer graphene (NGr) for a comparison. In the newly created composites, the ratio of oxide/carbon-containing materials was chosen to be 75/25 in order to be consistent with the systems produced during our previous works (Ayyubov 2021a; Vass 2019; Yazici 2021). Based on the analysis of the new types of support materials and supported Pt catalysts by physical-chemical characterization methods we attempted to find relationships between their structural, morphological properties and their electrocatalytic behavior. We identified the effects of the N-doping and the method of composite formation on

the microstructure of the catalysts. The electrochemical behavior of the catalysts was interpreted in terms of their microstructural peculiarities.

Experimental

Materials

Sodium hydroxide (NaOH, >98%) was product of Reanal, while concentrated nitric acid (cc. HNO_3, 65%, a.r.), 2-propanol (*i*-C_3H_5OH, 99.9 V/V%, a.r) ethylene-glycol (EG, 99.8%), sodium borohydride ($NaBH_4$, 99.95%) were purchased from of Molar Chemicals. Sulfuric acid (H_2SO_4, 96% p.a, Merck), hydrochloric acid (HCl, 36,4%, AnalaR NORMAPUR, VWR International) were also used. Hexachloroplatinic acid hexahydrate ($H_2PtCl_6 \times 6H_2O$, 37.5 % Pt) Pt precursor compound was purchased from Sigma-Aldrich. The gases (H_2, N_2, Ar) used in this work were products of Linde Gáz Magyarország Zrt. with 5.0 purity. Catalyst ink was prepared by use of 5% Nafion® dispersion (DuPont™ Nafion® PFSA Polymer Dispersions DE 520).

Titanium-isopropoxide (Ti(O-*i-Pr*)$_4$, Aldrich, 97%) was used as Ti precursor compound of the sol-gel prepared samples; P25 (Evonic) was used as starting TiO_2 for mechanochemical composite preparation. Graphite carbon rod (99.9%) and 2,4,6-triamino-1,3,5-triazine (melamine) precursors were purchased from Merck. GO was prepared from graphite by the Hummers-Offeman method. N-doped starting materials were prepared as we described earlier (Ayyubov 2021b). Briefly, in order to get NGO, GO dispersion was centrifuged to remove excess amount of water. Then ammonia (25%) was poured onto the GO dispersion, and the GO-ammonia mixture was sonicated to delaminate the GO sheets. After that, the solution was heated in a Teflon-sealed autoclave (160 °C for 12 h and at 180 °C for 2 h). Then the obtained solution was separated via centrifugation and the resulting solid was washed with water and ethanol.

NGr was prepared from graphite and melamine in a planetary ball milling machine (PM 400, Retsch Inc., Düsseldorf, Germany). Stainless-steel grinding jar together with 30 grinding balls was used at 400 rpm, room temperature (RT) for 24 h. Afterward, the material was washed with hot water to remove the un-reacted melamine. Finally, the sample was freeze dried. Based on XPS data surface N content of parent N-doped carbonaceous material was 8 atomic %, and 14 atomic % for NGO and NGr, respectively. The SSA_{BET} was 401 m^2/g and 37 m^2/g for NGO and NGr, respectively (Ayyubov 2022).

Preparation of composite supports and supported Pt electrocatalysts

Two different routes i.e. sol-gel (Borbáth 2021a) and mechanochemical ones (Ayyubov 2021b) were used for composite preparation.

In order to get 75 wt.% TiO_2 - 25 wt.% carbonaceous material type of composite supports a sol-gel synthesis was carried out by use of GO as N-free and NGO as N-containing starting carbonaceous materials. As we described earlier in case of GO (Ayyubov 2021a), a transparent acidic TiO_2 colloidal solution was made first by adding Ti(O-*i*-*Pr*)$_4$ into the vigorously stirred mixture of cc. HNO_3 and distilled water. The volumes of H_2O and cc. HNO_3 were calculated to adjust the concentration of Ti(O-*i*-Pr)$_4$ to 0.115 M and of HNO_3 to 0.69 M in the first step of the procedure (5 h stirring). Then desired amount of carbonaceous starting material was weighted. For exfoliation of it, NaOH solution (pH~ 14) was added to the suspension of the carbonaceous starting material till its pH became ~9. This suspension was sonicated for 25 min. Then the colloidal TiO_2 solution was poured into the carbonaceous suspension at once under vigorous stirring. After that aqueous HNO_3 solution (prepared from 0.4 mL cc. HNO_3 and 7.9 mL H_2O) was added into the slurry. The pH of the slurry was adjusted to that of TiO_2 sol with cc. HNO_3 and the reaction mixture was stirred continuously for 6 days at RT for aging in order to facilitate rutile nuclei formation. After six days of aging, the mixture was centrifuged. The solid part was washed three times with diluted nitric acid in order to remove the well soluble $NaNO_3$. Finally, the solid was re-suspended in diluted HNO_3 of the same volume. After the removal of $NaNO_3$, the slurry was evaporated at 65 °C and dried overnight in an oven at 85 °C. As a final step of the synthesis of the catalyst support material, a high temperature treatment (HTT) for 8 h at 600 °C in Ar atmosphere was performed to get well crystallized rutile TiO_2. These samples are denominated **75TiO2-25X-SG** (X: GO, NGO) (see Table 1).

Table 1. Denomination of electrocatalyst supports and result of the low temperature nitrogen physisorption measurements over them. Nominal TiO_2/C (N-C) weight ratio: 75/25

Sample ID	**Composite preparation method**	**Type of carbon source**	**Total pore volume, cm^3/g**	**SSA$_{BET}$, m^2/g**
75TiO2-25GO-SG[a]	Sol-gel	GO	0.69	264
75TiO2-25NGO-SG	Sol-gel	NGO[b]	0.20	109
75TiO2-25NGr-BM	Mechanochemical	NGr[c]	0.07	58

[a]from Ref. (Ayyubov 2021a); GO: graphite oxide, [b]NGO: N-doped graphite oxide described in Ref. (Ayyubov 2022); [b]NGr: N-doped multilayer graphene described in Ref. (Ayyubov 2022).

Beside the sol-gel method, a mechanochemical one by use of a planetary ball milling machine was also applied in order to prepare a composite of 75 wt.% TiO_2 - 25 wt.% N-C. First, P25 was heated at 1000 °C to get TiO_2 in rutile phase exclusively. After that, NGr and rutile-TiO_2 were loaded in a stainless-steel grinding jar with 30 grinding ball (10 nm diameter) and grinded for 24 h at 400 rpm at RT. Then, the obtained material was stirred in water for 5 minutes, filtrated, thoroughly washed with double distilled water and freeze dried. The above composite is denominated as **75TiO2-25NGr-BM** (Table 1).

The composite type of support materials were loaded with 20 wt.% Pt via a modified, sodium borohydride ($NaBH_4$) assisted ethylene-glycol (EG) reduction-precipitation method in order to obtain platinum containing electrocatalyst as we described before (see Ref. (Vass 2017)). Briefly, $H_2PtCl_6 \times 6H_2O$ (134 mg) was dissolved in ethanol in a round bottom flask. The 200 mg of the support material was dispersed in the solution by sonication at RT and the suspension was heated up to 65 °C with continuous stirring. A solution prepared by mixing of $NaBH_4$ (596 mg) and EG (7.4 mL) was added dropwise to the suspension very slowly and carefully with a syringe pump in 30 minutes at 65 °C with continuous stirring. After the addition of $NaBH_4$ and EG in 30 minutes the system was stirred at 65 °C for 3 hours. 0.2 M solution of hydrogen chloride (15 mL) was added to the suspension and it was stirred for an additional 2.5 hours at room temperature in order to allow the Pt particles to settle on the surface of the support. The material was washed four times with 50 ml water and filtered by centrifugation in order to remove the chloride ions and dried at 85 °C in an oven overnight.

Structural and surface analysis of supports and supported Pt electrocatalysts

Nitrogen physisorption measurements were carried out at temperature of liquid nitrogen using Thermo Scientific Surfer automatic volumetric adsorption analyzer (Thermo Fischer Scientific, Berlin, Germany). The specific surface was calculated by the BET method (SSA_{BET}) in the range of relative pressures from 0.05 to 0.30.

XRD patterns were obtained in a Philips model PW 3710 based PW 1050 Bragg-Brentano parafocusing goniometer using CuKα radiation (λ= 0.15418 nm), graphite monochromator and proportional counter. The average crystallite size of Pt (Salgado 2010) and TiO_2 was determined from fitted data by means of Scherrer formula (Patterson 1939).

XPS measurements were performed using an electron spectrometer manufactured by OMICRON Nanotechnology GmbH (Germany). MgKα (1253.6 eV) radiation was used as excitation source and data were acquired with 1 eV spectral resolution (30 eV pass energy). The

powdered composite supports and catalysts were suspended in isopropanol and drops of this suspension were dried onto stainless steel sample plates. Spectra were processed with the CasaXPS package (Fairley 2006) by fitting the measured data with a combination of Gaussian-Lorentzian product peaks over a Shirley-type background, while quantitative evaluation of the data was performed with the XPSMultiQuant package (Mohai 2004, 2011) during which a homogeneous depth distribution was assumed for all components. Chemical states were identified using the NIST database (Wagner 2003), the publication (Moulder 1992) or other literature as indicated. Binding energies were referenced to the lowest binding energy contribution of the C 1s envelope, which was assigned to graphite-like (sp^2-hybridized) carbon in the carbon backbone (284.4 eV).

Morphology of the electrocatalysts was investigated by TEM in HRTEM and STEM HAADF modes by means of a FEI Titan Themis 200 kV Cs - corrected TEM with 0.09 nm HRTEM and 0.16 nm STEM resolution. Composition of the samples was measured by STEM-EDS.

The conductivity of the powdery electrocatalysts was measured using a home-made two-probe instrument completed by a potentiostat (BioLogic) in a two-electrode cell setup via potentiostatic electrochemical impedance spectroscopy (PEIS) in the frequency range of 1 mHz – 10000 kHz. In order to check the accuracy of the setup the conductivity tests of BP and Vulcan XC-72 carbon black powders were measured.

Electrochemical characterization

The details of the electrochemical characterization including the preparation of working electrode, the composition of catalyst ink and electrocatalytic measurements were described in Refs. (Borbáth 2021a; Vass 2017; Vass 2018). The measurements were done in a standard three-electrode cell using 0.5 M H_2SO_4 electrolyte solution. Glassy carbon (surface area: 0.0707 cm^2) was used as working electrode, platinum wire as counter electrode and a hydrogen electrode as reference electrode. All potentials are given on the reversible hydrogen electrode (RHE) scale.

Due to the low electronic conductivity of the **Pt/75TiO2-25NGO-SG** sample, an increase in conductivity was achieved by preparing a mechanical mixture of the original catalysts with 20 wt.% BP carbon (BP: Black Pearls 2000 (CABOT)). For this purpose, the sample was mixed in a mortar with carbon in a mass ratio of 80/20; sample homogeneity was ensured by rotating using a tube rotator (VWR) for 24 hours. Mechanical mixture of NGO-

containing catalyst with BP was denominated as **Pt/75TiO2-25NGO-SG-BP**. The Pt loading of the electrodes was 8.2 and 10.2 μg cm^{-2} for the catalysts used with and without addition of 20 wt.% BP carbon, respectively.

Electrocatalytic performance of the 20 wt.% Pt/TiO_2-C(N-C) electrocatalysts was studied by cyclic voltammetry combined with stability test involving 500 polarization cycles and ORR measurements. ORR activity of the catalyst samples in O_2 saturated 0.5 M H_2SO_4 solution was tested by rotating disc electrode (RDE) technique (for details see Borbáth 2021b).

Results

Structural characterisation of supports and supported Pt catalysts

The results of the low temperature N_2 physisorption measurements (see Table 1) showed that the sol-gel method resulted in SSA_{BET} of the composite supports larger than 100 m^2/g regardless of type of carbonaceous material, although using NGO instead GO led to both smaller SSA and pore volume. However, the sample obtained by the mechanochemical way (**75TiO2-25NGr-BM**) did not reach the recommended value of SSA_{BET} (100 m^2/g) (Zhang, Z. 2014). In accordance with literature findings (Gohari-Bajestani 2017; Hou 2022), the total pore volume and SSA_{BET} of our TiO_2-(N-C) type of composites are smaller than that of their TiO_2-C counterpart. In case of the sol-gel prepared sample the probable reason of this phenomenon is the decreased amount of functional groups of NGO starting material compared to GO, the parent material of the N-doped carbon. The mechanochemically prepared sample, **75TiO2-25NGr-BM** have the smallest total pore volume and SSA_{BET} in the series of our composites indicating that our grinding method was less effective.

The results of the XRD characterisation of Pt catalysts supported by the different composites are presented in Figure 1 and Table 2.

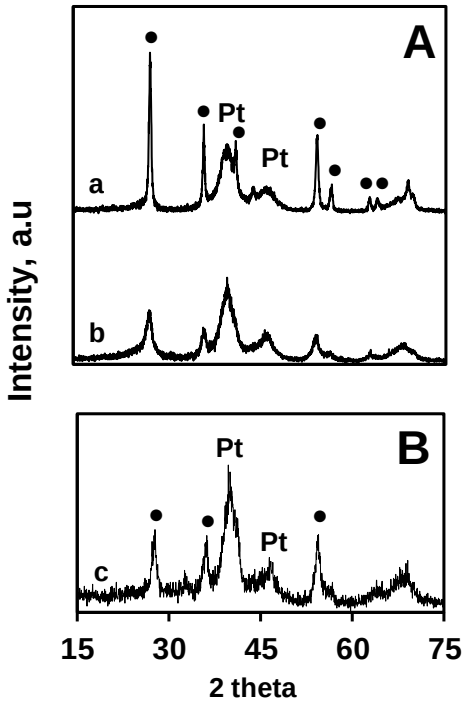

Figure 1. XRD pattern of various composite supported Pt electrocatalysts. A: sol-gel prepared samples (line a: **Pt/75TiO2-25GO-SG**, line b: **Pt/75TiO2-25NGO-SG**) B: mechanochemically prepared **Pt/75TiO2-25NGr-BM** sample. ●-rutile

Table 2. Characterization of the Pt/TiO_2-C catalysts (nominal Pt content: 20 wt.%; nominal value of TiO_2/C (N-C): 75 wt.%/25 wt.%)

Sample ID	XRD average crystallite size, nm		XPS, wt.%/wt.%	
	Pt	TiO_2[b]	TiO_2/C	Pt/support
Pt/75TiO2-25GO-SG[a]	2.9	16.0	55/45[c]	47/53
Pt/75TiO2-25NGO-SG	3.0	6.4	84/16[c]	73/27
Pt/75TiO2-25NGr-BM	3.1	7.7	48/52[c,d]	63/37

[a]from Ref. (Ayyubov 2021a); [b]TiO_2 existed exclusively in rutile phase; [c]calculated without Pt; [d]calculated without iron oxide; Ti and iron oxides together give an oxide/carbon weight ratio of 67/33

The characteristic peak of Pt (JCPDS card 00-004-0802) can be observed at 2θ = 40° which corresponds to the (111) reflection plane. The broad band of Pt in the XRD patterns (Figure 1) indicated the presence of the Pt in highly dispersed form in all samples as has been confirmed by TEM in our previous work (Borbáth 2021a). Scherrer's equation (Patterson 1939) was used in order to estimate the average crystallite size from XRD data and the (220) peak of the Pt fcc structure around 2θ =70◦ was chosen. This region was chosen to avoid the influence of a broad band of the carbon substrate and rutile on the (111) and (200) peaks of Pt structure (Salgado 2010). The average crystallite sizes of Pt calculated were very close to each other around 3.0 nm (Table 2). Fine dispersion of Pt was mainly related to the applied reduction-

deposition method and to a lesser extent depended on the structural characteristics of the support (Borbáth 2021a). A bit smaller values were found by TEM for our Pt/mixed oxide - carbon systems in our previous studies (Borbáth 2021a; Vass 2017). XRD results proved that TiO_2 existed in all samples in the desirable rutile phase. The most intensive reflections of rutile TiO_2 at $2\theta = 27.5°$ (110), at $2\theta = 36.1°$ (101), at $2\theta = 54.4°$ (211) and at $2\theta = 56.7°$ (220) according to the JCPDS Card no.21-1276 can be observed in case of all the tree composites while the most characteristic reflection for anatase TiO_2 at $2\theta = 25.3°$ (101) according to JCPDS Card no. 21-1272 cannot be found (Figure 1). The composite prepared from GO showed the sharpest reflections (line a in Figure 1A) of rutile suggesting a higher degree of the crystallization of TiO_2 in this composite. The calculated average crystallite size of TiO_2 of N-free **Pt/75TiO2-25GO-SG** was significantly higher than that of the other samples prepared by use of N-C (see Table 2). The average particle size of rutile of the mechanochemically prepared sample was smaller than in the commercial P25 (45 nm (Majrik 2018)) as a combined result of the opposing effects of preliminary heat treatment and grinding. In respect of the carbonaceous part of the composites, characteristic reflection of the parent GO at $2\theta = 12.9°$ (Mastalir 2012) cannot be observed in the XRD pattern of the sample **Pt/75TiO2-25GO-SG** (not shown). The NGO starting material showed a slightly intense, broad band with a maximum around $2\theta \sim 24\text{-}25°$ (Ayyubov 2022), which, however, cannot be separated in the XRD profile of **Pt/75TiO2-25NGO-SG** composite (Figure 1A, line b). The characteristic reflection of the parent graphite (002) at $2\theta = 26.6°$ was absent in the XRD pattern of the mechanochemically prepared sample ((Figure 1B, line c). The latter findings suggest that the carbon component of the composites underwent a significant change during the preparation of the composites.

Surface and morphological characterisation of supported Pt catalysts

Regarding the surface of the composite supported catalysts, the most important composition data measured by XPS were summarized in Table 2, while binding energies of the most characteristic peaks of the components can be found in Table 3.

The Pt/support ratio deduced from XPS was in all cases much higher than the nominal value (Table 2), indicating that the microstructure of the catalysts was inhomogeneous at the length scale of XPS. In particular, the high apparent Pt content measured by XPS can be explained by the location of the Pt on the outer surface of relatively large support grains. In line with the XRD studies, XPS results confirmed that the vast majority of Pt was present in metallic form, as indicated by the 71.2-71.3 eV binding energy of the dominant Pt $4f_{7/2}$ component

(Naumkin 2023). A minimal ionic Pt contribution showed the presence of trace amounts of Pt oxides due to surface oxidation.

A general feature of the TiO_2- or Mo-doped TiO_2-carbon composites prepared by the sol-gel method is that the apparent oxide content determined by XPS is lower than the nominal value. It is the result of the relatively weak interaction between titania and the carbon backbone, which leads to growth of large flower-like oxide agglomerates during high temperature treatment (Ayyubov 2021a; Borbáth 2021a). This behavior is reproduced in case of the **Pt/75TiO2-25GO-SG**, while the much higher oxide/carbon ratio of **Pt/75TiO2-25NGO-SG**, along with its diminished oxide particle size, suggests a much more homogeneous coverage of the carbon by TiO_2.

Binding energies of the Ti $2p_{3/2}$ peak indicated the exclusive presence of Ti^{4+} (completely oxidized Ti) in all catalysts (NIST data base (Naumkin 2023)).

C 1s spectrum of **Pt/75TiO2-25GO-SG** was dominated by graphitic carbon signals as the result of reduction of GO during the synthesis, as described in (Ayyubov 2021a); small additional peaks appearing around 286 and 288 eV binding energies arose from O- containing functional groups (Mohai 2018; Stobinski 2012; Wang, H. 2012; Yamada 2013). The graphite-like features were less obvious in the quite weak C 1s spectrum of **Pt/75TiO2-25NGO-SG**; this fact, together with the relatively high oxide content (Table 2) indicated the much better coverage of the oxide over the carbonaceous backbone in this system. A slight shift of the main C 1s peak towards higher binding energies and the disappearance of the graphitic features in the C 1s line shape of **Pt/75TiO2-25NGr-BM** suggested destroying of the graphitic structure during the ball milling synthesis, while the O- or N-containing functional groups remained still present.

Table 3. Binding energies and assignments of the most important photoelectron peaks of the Pt/TiO_2-C catalysts

Peak	**Sample/Binding energy (eV)**			**Assignment**
	Pt/75TiO2-25GO-SG[a]	**Pt/75TiO2-25NGO-SG**	**Pt/75TiO2-25NGr-BM**	
Pt $4f_{7/2}$	71.2 72.5	71.3 74.8	71.3 72.6 74.8	metallic Pt [b] Pt^{2+}: PtO [b] (very small) Pt^{4+}: PtO_2 [b] (very small)
Ti $2p_{3/2}$	458.9	459.0	458.3	Ti^{4+}: TiO_2 [b]
C 1s	284.4 285.9 288.2	284.6 286.5 289.1	284.6 286.2 288.0	graphitic C, sp^3 carbon [b] (main peak) C-OH, C-NH_x, epoxide [c,d,e,f] (weak) carbonyl, carboxyl, C-N-C [f] (weak)
O 1s	530.2	530.3	529.8	metal oxide [b] (TiO_2, FeO_x, main peak)

	531.9 533.2 535.7	532.2 535.0	531.4 533.1 535.0	-OH on metal oxide [g], epoxide [c,d] -OH on C, carboxyl [c,d] (weak) adsorbed moisture [b]
N 1s	-	 399.5	398.3 399.4 405.0	pyridinic N [h] pyrrolic N [h] oxidized N [h]
Fe $2p_{3/2}$	-	-	711.0	Fe^{3+}: Fe_2O_3, FeOOH [b]

[a] from Ref. (Ayyubov 2021a)
[b] (Naumkin 2023)
[c] (Stobinski 2012)
[d] (Yamada 2013)
[e] (Wang, H. 2012)
[f] (Mohai 2018)
[g] (Hugenschmidt 1994)
[h] (Dan 2021)

A peculiarity of the **Pt/75TiO2-25NGr-BM** sample was the appearance of the iron in relatively high quantity (5 atomic% or 7 wt.%, TiO_2:FeO_x weight ratio around 1:1.2) on the surface of the catalyst due to the hardness of TiO_2 and the stainless grinding jar and balls. According to XPS, the iron content was completely oxidized. The presence of Fe was confirmed by inductively coupled plasma - optical emission spectrometry (ICP-OES) technique after microwave assisted dissolution; the amount (7.8 wt.%) was comparable to that measured by XPS.

The O 1s spectra of the samples were dominated by signals from TiO_2 (or mixture of TiO_2-iron-oxide in **Pt/75TiO2-25NGr-BM**) around 530 eV binding energy, while the tail of the spectrum towards higher binding energies contained contributions from both the oxide (like -OH groups on the oxide, giving a peak around 531.5-532 eV (Hugenschmidt 1994) or the oxygen-containing functional groups of the carbon (Stobinski 2012; Yamada 2013).

Because of the good oxide coverage, only a minimal, broad N 1s peak was observed in **Pt/75TiO2-25NGO-SG**. In the N 1s spectrum of **Pt/75TiO2-25NGr-BM** pyridinic, pyrrolic and oxidized N contributions were identified, as described in detail in (Ayyubov 2022).

TEM images of sol-gel prepared samples are presented in Figure 2.

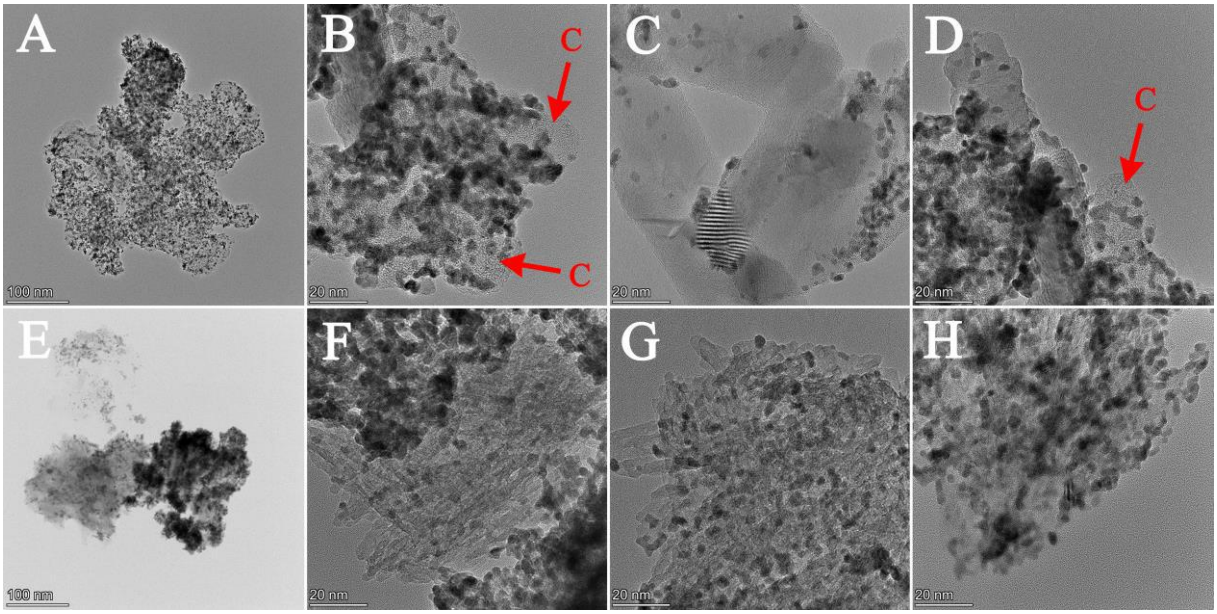

Figure 2. TEM images of various Pt electrocatalyst supported by sol-gel prepared composites: **Pt/75TiO2-25GO-SG** (A, B, C, D) and **Pt/75TiO2-25NGO-SG** (E, F, G, H). Onion-like carbon structures in B and C are highlighted by arrows and letter C.

In accordance with the XRD and XPS results, finely dispersed Pt existed on all samples due to the use of $NaBH_4$ assisted EG reduction precipitation method. In line with the results of the quantitative XPS investigation, the GO derived sample (**Pt/75TiO2-25GO-SG**) contained TiO_2 in the form of both small and significantly larger crystals (Figure 2ABCD) as we observed earlier in case of composite supported catalysts containing TiO_2 (Ayyubov 2021a) and Ti-Mo mixed oxides (Borbáth 2021a). It is worth noting that the GO derived sample showed uncovered carbonaceous surfaces (onion like patterns in Figures 2B and 2D, emphasized by arrows and letter C), too. However, TEM images of the NGO derived sample were conspicuously different from those of its GO counterpart (cf. Figure 2ABCD and Figure 2EFGH). Sample **Pt/75TiO2-25NGO-SG** contained TiO_2 in the form of elongated, small rutile crystals in accordance with the average crystallite size calculated from the XRD results. The TiO_2 coverage was even and the presence of "empty" carbonaceous part was not characteristic in this sample.

Use of NGr and high ratio of TiO_2 by ball milling led to robust particles (Figure 3ABCD). This texture was reflected in the very low SSA_{BET} of the **75TiO2-25NGr-BM** support (see in Table 1). In the large particles rutile features were clearly observed (along with crystalline metallic Pt, Figure 3 A-C), while carbon-looking structures, still associated with rutile, were only rarely seen (Figure 3 D).

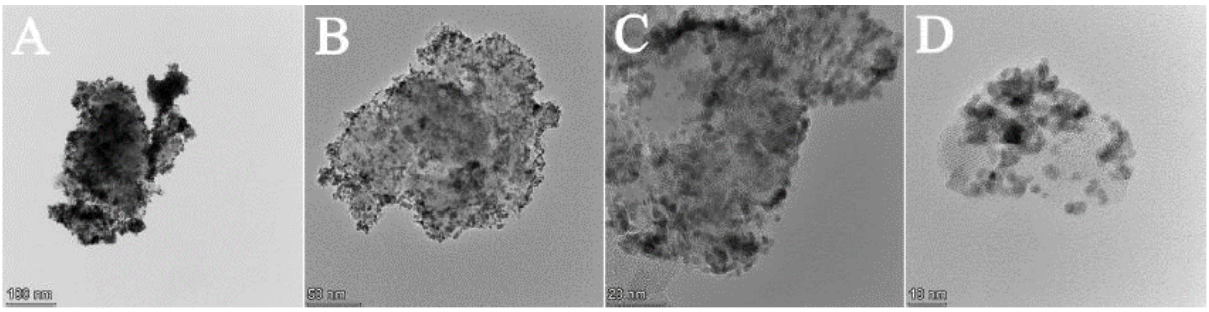

Figure 3. TEM images of Pt electrocatalyst supported by mechanochemically prepared composite (**Pt/75TiO2-25NGr-BM**). Toolbar: 100 nm (A), 50 nm (B), 20 nm (C), 10 nm (D)

The significant differences between the elemental map of GO derived catalyst and that of NGO derived one could be seen (Figure 4), too.

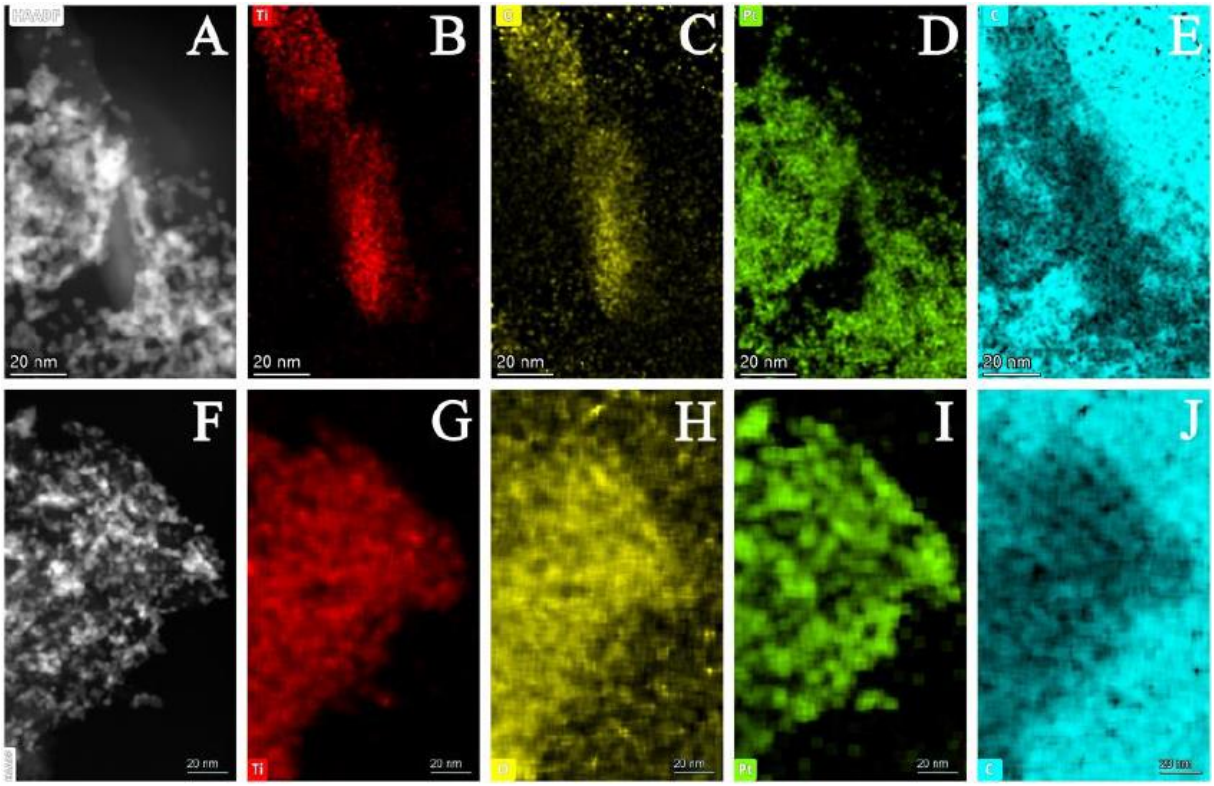

Figure 4. Elemental maps of Pt electrocatalyst supported by sol-gel prepared composites: **Pt/75TiO2-25GO-SG** (A, B, C, D, E); **Pt/75TiO2-25NGO-SG** (F, G, H, I, J). Toolbars: 20 nm

While the GO derived catalyst had Pt covered carbon- and Pt covered TiO_2 parts (Figure 4BDE) element maps of Ti, Pt and C were completely congruent in the NGO derived catalyst (cf. Figure 4GIJ). The pattern of O-map was very similar to that of Ti-map in both samples (cf. Figure BC and Figure 4 GH). This finding confirmed the picture suggested by XPS and observed on TEM images, i.e. the surface of **Pt/75TiO2-25NGO-SG** sample was almost completely covered with TiO_2.

Elemental maps of the catalyst supported by the composite obtained from mechanochemical way (**Pt/75TiO2-25NGr-BM**) are showed in Figure 5. As can be seen in Figure 5D, Pt concentrated at the edge of the particles which was in line with the high Pt/support ratio detected by XPS on the surface.

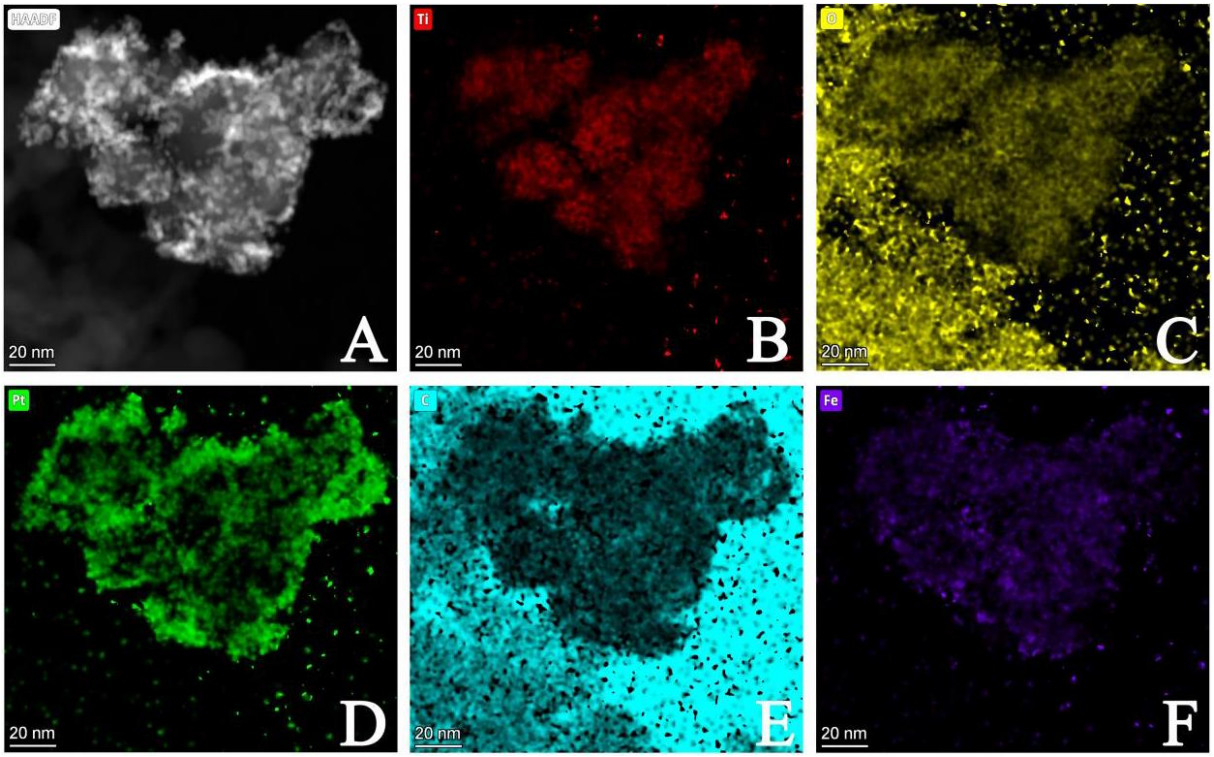

Figure 5. Elemental maps of Pt electrocatalyst supported by ball-milling prepared composite (**Pt/75TiO2-25NGr-BM).** Toolbars: 20 nm

Elemental mapping of catalyst **Pt/75TiO2-25NGr-BM** also proved the presence of Fe in this sample (Figure 5F) which was also indicated by XPS and ICP-OES. However, Fe was not detected in the other two samples, for which the support was prepared by sol-gel method.

Electrical conductivity of supported Pt catalysts

Results of the electrical conductivity measurements of the catalysts are presented in Figure 6.

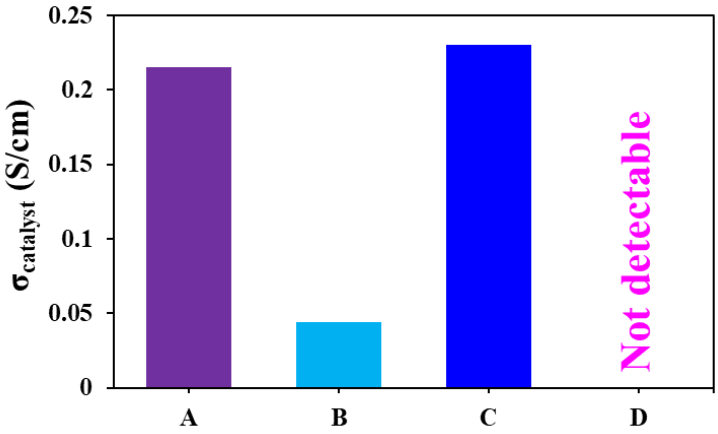

Figure 6. Results of electrical conductivity measurements of various Pt/TiO_2-C samples. A: **Pt/75TiO2-25GO-SG** (), B: **Pt/75TiO2-25NGO-SG** (), C: **Pt/75TiO2-25NGO-SG-BP** () and D: **Pt/75TiO2-25NGr-BM** ().

Although the conductivity of the GO derived catalyst **(Pt/75TiO2-25GO-SG)** measured by our home-made equipment during standardized conditions, was two orders of magnitude less than that of the commercial 20 wt.% Pt/C (Quintech) (0.22 S/cm versus 22 S/cm), it showed outstanding value compared to N-containing composite supported samples. As shown in Figure 6, N-C-containing sol-gel and ball-milling synthesized catalysts had very low conductivity or had "insulator" character having no detectable conductivity. In case of **Pt/75TiO2-25NGO-SG** this behavior can be explained by the almost complete TiO_2 cover of the carbonaceous backbone indicated by the very high TiO_2/N-C ratio on the surface obtained from XPS data (Table 2), furthermore confirmed by TEM images (Figure 2) and elemental maps (Figure 4). Mechanical mixing of the catalyst with Black Pearls 2000 significantly improved the situation. Similarly, in case of the **Pt/75TiO2-25NGr-BM** catalyst the insulating nature was most probably the consequence of the lack of the extended carbonaceous backbone.

Electrochemical behavior of supported Pt catalysts

Cyclic voltammograms (CVs) obtained in the 1st and 500th cycles of the stability test of Pt electrocatalysts supported on the composites prepared in this study are presented in Figure 7.

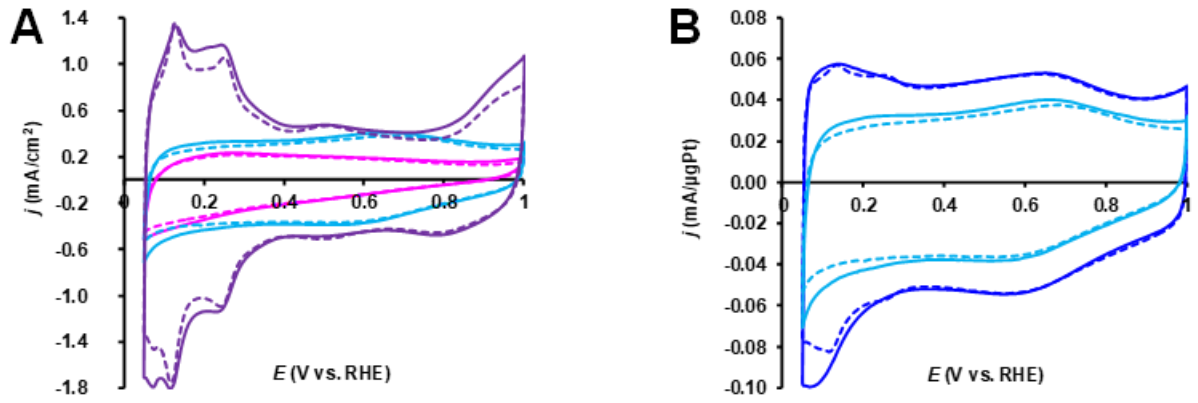

Figure 7. Cyclic voltammograms of various composite supported Pt electrocatalysts obtained before and after 500-cycle stability test: **Pt/75TiO2-25GO-SG** (), **Pt/75TiO2-25NGO-SG** (), **Pt/75TiO2-25NGr-BM** () and **Pt/75TiO2-25NGO-SG-BP** (). The current was normalized to the geometric surface area (A) and Pt loading of the electrode (B). The voltammograms were recorded in 0.5 M H_2SO_4 at 100 mV s^{-1} sweep rate and T = 25 °C. Solid line: 1st cycle; dashed line: 500th cycle.

It can be seen that the support significantly affects the shape of the CVs. Only on the N-free GO-containing **Pt/75TiO2-25GO-SG** catalyst was observed a typical CV of Pt with the classical features of the adsorption/desorption of underpotentially deposited hydrogen between 50 and 350 mV and platinum oxidation/reduction peaks above 700 mV (Figure 7A), similar to those described in the literature and our own studies (Borbáth 2021a; Huang, S. Y. 2011; Vass 2017). However, the CVs of the N-containing samples were completely different (Figure 7A): instead of the characteristic features of Pt-containing systems, the voltammograms resembled those reported in the literature for Pt-free TiO_2 and/or N-C-containing catalysts (El-Deen 2015; Kang 2014; Li 2019; Sundriyal 2018; Thakur 2018). It is important to mention that the shape of the CV curves of sol-gel and mechanochemically prepared, N-doped carbon containing catalysts (Figure 7A) also differ from each other. The larger double layer (DL) capacitance, obvious broad anodic and cathodic redox peaks ranged from 0.4 to 0.8 V (vs. RHE) observed in the CV of **Pt/75TiO2-25NGO-SG** catalyst suggests that the synthesis procedure (sol-gel or ball-milling) used for preparation of the support materials has an effect on the electrochemical performance of the catalysts.

An explanation for the larger double layer (DL) capacitance could be that the underlying NGO- surface with high functionality compared to NGr carbon (Ayyubov 2022; Li 2019). Above phenomenon is often related to the pseudocapacitance introduced by the redox reactions of N- and O-containing functionalities, since it is known that heteroatom doping on the graphene sheet may lead to the appearance of such pseudocapacitance on a graphene network (Balaji 2020; Li 2019). However, only negligible N was detected by XPS on the surface of

Pt/75TiO2-25NGO-SG catalyst compared to the mechanochemically prepared sample (**Pt/75TiO2-25NGr-BM**) and our XPS and TEM results suggested that the carbonaceous part of the **Pt/75TiO2-25NGO-SG** is mainly covered by the oxide. Therefore, we believe that an another explanation is more probable, i.e. mainly the insulating nature of the support is responsible for the lack of the characteristic Pt features. The importance of close contact between Pt and the conductive support, allowing the catalyst to exhibit the typical electrochemical activity of Pt in CVs, has been already highlighted in numerous literatures on this subject (Bauer 2010; Takabatake 2014). To increase the conductivity of oxide-containing supports, several methods have been proposed. For instance, in the case of TiO_2-containing catalysts, it has been demonstrated (Huang, K. 2012) that after doping with carbon, the c-TiO_2/CNT support has a significantly higher electrical conductivity than undoped TiO_2/CNT, which was manifested in the appearance on the CVs of Pt electrocatalysts corresponding peaks in the regions of hydrogen adsorption/desorption, platinum oxidation, and platinum-oxide reduction.

One of the simplest ways to improve conductivity of the oxide-containing catalysts is to prepare mechanical mixtures of these materials with carbon (e.g., (Micoud 2009; Somacescu 2023; Wang, D. 2010)). CVs of the NGO derived composite supported catalyst obtained with (**Pt/75TiO2-25NGO-SG-BP**) and without addition (**Pt/75TiO2-25NGO-SG**) of 20 wt.% BP carbon are presented in Figure 7B. As expected, the addition of carbon leads to an increase in capacitance compared to the original sample due to better access of the electrolyte to the electrode surface. After 500-cycle stability test for the catalyst mixed with carbon some increase of the peak associated with adsorption/desorption of underpotentially deposited hydrogen (H_{upd}) on Pt surface was observed. Moreover, as shown in Figure 7, both N-containing samples have higher stability compared to N-free **Pt/75TiO2-25GO-SG** catalyst.

The results of the investigation of the ORR are depicted in Figure 8. It is clearly visible that among the catalysts studied only the N-free GO derived one had significant activity in this reaction. As shown in Figure 8, N-containing catalysts used without mixing with carbon had much lower activity, since the ORR linear sweep voltammetry curves did not even reach the plateau region in the selected potential window.

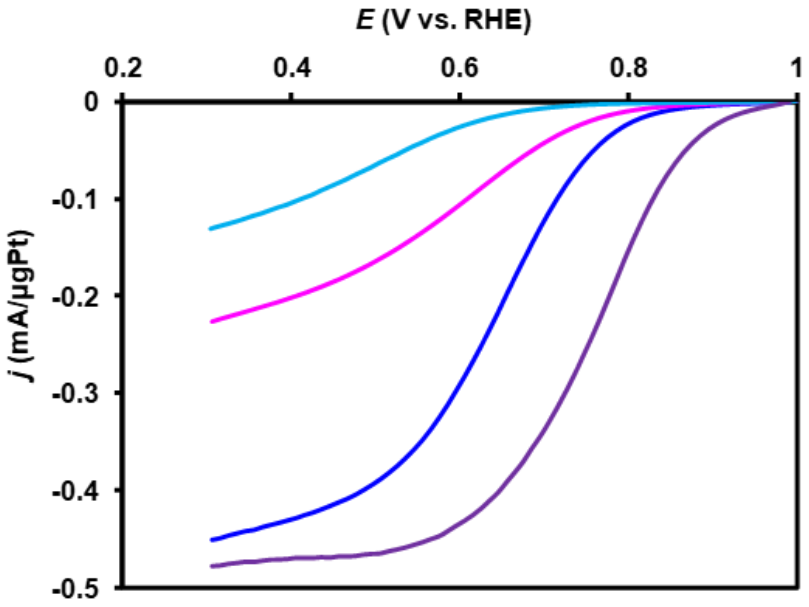

Figure 8. ORR curves obtained on fresh composite supported Pt electrocatalysts in O_2-saturated 0.5 M H_2SO_4 on a RDE at 1600 revolutions/min (rpm) recorded at 10 mV s^{-1} sweep rate and 25 °C: **Pt/75TiO2-25GO-SG** (), **Pt/75TiO2-25NGO-SG** (), **Pt/75TiO2-25NGO-SG-BP** () and **Pt/75TiO2-25NGr-BM** (). The Pt loading of the electrodes was 8.2 and 10.2 µg cm^{-2} for the catalysts used with and without addition of 20 wt.% BP carbon, respectively.

However, as shown in Figure 8, a sharp increase in activity was observed after mixing the NGO-containing catalyst with carbon. As can be seen from in Figure 8, the onset potential for the ORR was increased in the following order: Pt/75TiO2-25NGO-SG (790 mV) < Pt/75TiO2-25NGr-BM (870 mV) < Pt/75TiO2-25NGO-SG-BP (890 mV) < Pt/75TiO2-25GO-SG (950 mV).

Discussion

From the comparison of the XRD, XPS and TEM results obtained on samples prepared by the sol-gel method, it could be concluded that N-doping of GO strongly influenced the crystallization of the TiO_2 in the composite. While both small and large TiO_2 crystals appeared in the N-free system, the TEM image showed only small, elongated crystals in the case of the NGO backbone. At the same time, Ti and C elemental maps showed almost complete cover of N-C with TiO_2, while N-free composite had non-covered carbonaceous parts. too. Using the same nominal ratios of TiO_2/C (N-C), it is evident that that smaller rutile crystallites could form more complete TiO_2 cover if the SSA_{BET} of the starting carbonaceous materials were equal or less. It has been known from our previous work that the specific surface area of the carbon material and the nominal oxide/C ratio also plays an important role in the morphology of the

TiO_2-based mixed oxides. During the use of various N-free carbonaceous materials (BP, Vulcan XC-72, GO) for preparation of composites, we have showed that carbon acts as a template, the SSA_{BET} of the composite support is also lower in case of carbon of small SSA_{BET}. Besides, the formation of giant, flower-like oxide formations are more likely when SSA_{BET} is low and nominal ratio TiO_2/C is high. However, there were no such formations when NGO was used, despite the high TiO_2/N-C ratio. In contrast, a uniform oxide coverage occurred, which could be attributed to the nucleating effect of N-sites.

As Pt was loaded on the support in the subsequent step of preparation, it was deposited practically to the top of TiO_2 in case of the NGO-based composite. As a result, the possibility of formation of C-Pt or C-Pt-Ti junctions was very low in the **Pt/75TiO2-25NGO-SG** catalyst. In contrast, formation of Pt-TiO_2-C connections on the GO-containing sample is more probable, which is favorable from the point of view of both Pt stabilization and electron transfer.

A strong relationship could also be found between the structure of the composites and the macroscopic electrical conductivity of the catalysts prepared from them. The finding that N-C-containing sol-gel type of catalyst had very low conductivity also could be the result of the almost complete TiO_2 cover of the carbonaceous backbone indicated by the very high TiO_2/N-C ratio on the surface (Table 2), confirmed by TEM images (Figure 2) and elemental maps (Figure 4). The shape of the CVs or the activity in ORR were consistent with the observation that the conductivity of this material was very low.

Interestingly, increasing the conductivity of **Pt/75TiO2-25NGO-SG** by physical mixing with carbon resulted in very significant increase of the ORR activity, while the electrochemical availability of Pt (as judged from the CVs) still remained much lower than that in **Pt/75TiO2-25GO-SG**. This observation suggests that the effect of N on the dispersion of TiO_2 can be beneficially utilized in development of high performance composite support systems, although further investigations must focus on development of materials in which the TiO_2/N-C ratio is much lower compared to the 75/25 weight ratio used in this work.

It can be summarized that the given N-doping concentration was not optimal for the composite with 75 wt.% of TiO_2. One option is to decrease the N content, however, we believe that decreasing the TiO_2/N-C ratio is the more promising way. To determine the optimum, we need to prepare a series of composites with different TiO_2/N-C ratios in our future works.

The mechanochemical method previously proved to be excellent for the production of N-doped graphite material. Although the method seemed simpler and more environmentally friendly for the preparation of composites than the sol-gel route, several problems appeared in the procedure we used. One of them is the very low specific surface area of the composite

substrate. The other problem to be eliminated was the appearance of Fe on the surface of the composite, presumably as the result of abrasion by the hard TiO_2 particles. The presence of Fe can make the surface processes more complicated during the polarization cycles and is believed to be disadvantageous. Moreover, the significant amount of Fe-oxide, along with the lack of a continuous carbonaceous network in the catalyst resulted in an insulating system. While preparation of higher surface area materials can be attempted by optimizing the grinding conditions, a more resistant grinding device is needed for avoiding the iron contamination.

5. Conclusion

Both N-doped carbonaceous materials and Pt-loaded oxide-carbon composites represent emerging classes of electrocatalytic materials proposed for application in polymer electrolyte membrane fuel cells. The aim of the present study was to explore whether N-doped carbons can be used as the carbonaceous component of the oxide-carbon composite support, which could allow the investigation of potential synergistic effects between them.

For the production of composite supports for electrocatalysts with 20 wt.% Pt content, we compared a sol-gel route using N-free and N-containing graphite oxide-based carbonaceous materials and a fully mechanochemical approach, which allowed significant N-doping of the carbonaceous component. We found that N-doping strongly influences the growth of TiO_2 on GO, forming an almost continuous coating of small TiO_2 crystals. While this TiO_2 coating is a prerequisite for maximizing Pt-oxide interactions, it acted as a quasi-insulating layer between the Pt catalytic sites and the conductive part of the composite, thusthe electrochemical activity of the catalyst was low. Nevertheless, the significant increase of the activity in ORR achieved after improving the conductivity of the catalyst by its physical mixing with carbon suggested that the effect of N on the dispersion of TiO_2 can be beneficially exploited for optimizing the number of the catalytically relevant Pt-oxide-C(N-C) ensemble sites if the oxide/carbon ratio of the composite is carefully chosen.

The main problems of the composite supports prepared by the mechanochemical way were the small specific surface area, the significant amount of Fe contamination, and, as their combined consequence, the insulating nature of the catalyst, which necessitates the optimization of our method.

Competing interest

The authors declare no conflict of interest. The funders had no role in the design of the study; in the collection, analyses, or interpretation of the data; in the writing of the manuscript; or in the decision to publish the results.

Funding

This research was funded by Project no. RRF-2.3.1-21-2022-00009, titled National Laboratory for Renewable Energy has been implemented with the support provided by the Recovery and Resilience Facility of the European Union within the framework of Programme Széchenyi Plan Plus. Financial support in the frame of VEKOP-2.3.3–15- 2016–00002 is greatly appreciated (Erzsébet Dodony).

Authors contribution

The contributions of the co-authors are the following:
Conceptualization, **Emília Tálas**; Methodology, **Emília Tálas** and **Irina Borbáth**; Catalyst preparation, **Ilgar Ayyubov** and **Camelia Berghian-Grosan,** Investigation of electrocatalytic reactions, XRD measurements, **Ilgar Ayyubov**; Investigation by TEM, **Erzsébet Dodony**; Investigation by XPS, **Zoltán Pászti**; Investigation by low temperature nitrogen physisorption, **Ágnes Szegedi**; Writing-Original Draft Preparation, **Emília Tálas**, **Zoltán Pászti** and **Irina Borbáth**; Supervision, **Adriana Vulcu** and **András Tompos**; Funding Acquisition: **András Tompos**. All authors have read and agreed to the published version of the manuscript.

Acknowledgement

The authors thank Tamás Szabó for providing graphite oxide, Anett Lázár for XRD-, and Zoltán May for ICP-OES measurements.

References

Antolini, E. 2012. Graphene as a new carbon support for low-temperature fuel cell catalysts. Applied Catalysis B: Environmental 123–124: 52–68. https://doi.org/10.1016/j.apcatb.2012.04.022

Ayyubov, I., I. Borbáth, Z. Pászti, Z. Sebestyén, J. Mihály, T. Szabó, E. Illés, A. Domján, M.

Florea, D. Radu, A. Kuncser, A. Tompos and E. Tálas. 2021a. Synthesis and Characterization of Graphite Oxide Derived TiO_2-Carbon Composites as Potential Electrocatalyst Supports. Topics in Catalysis No. 0123456789 https://doi.org/10.1007/s11244-021-01513-1

Ayyubov, I., A. Vulcu, C. Berghian-Grosan, E. Tálas, I. Borbáth, I. E. Sajó, G. Sáfrán, J. Mihály and A. Tompos. 2021b. Preparation of Pt electrocatalyst supported by novel, $Ti_{(1-x)}Mo_xO_2$-C type of composites containing multi-layer graphene. Reaction Kinetics, Mechanisms and Catalysis 135(1): 49–69. https://doi.org/10.1007/s11144-021-02138-x

Ayyubov, I., E. Tálas, C. Berghian-Grosan, L. Románszki, I. Borbáth, Z. Pászti, Á. Szegedi, J. Mihály, A. Vulcu and A. Tompos. 2022. Nitrogen doped carbonaceous materials as platinum free cathode electrocatalysts for oxygen reduction reaction (ORR). Reaction Kinetics, Mechanisms and Catalysis 136(1): 125–147. https://doi.org/10.1007/s11144-022-02331-6

Balaji, S. S., A. G. K. Raj, M. Karnan and M. Sathish. 2020. Investigations on the nature of electrolyte on the electrochemical supercapacitor performance of heteroatom doped graphene. Ionics 26(4): 2081–2094. https://doi.org/10.1007/s11581-020-03448-1

Bauer, A., K. Lee, C. Song, Y. Xie, J. Zhang and R. Hui. 2010. Pt nanoparticles deposited on TiO_2 based nanofibers: Electrochemical stability and oxygen reduction activity. Journal of Power Sources 195(10): 3105–3110. https://doi.org/10.1016/j.jpowsour.2009.11.107

Borbáth, I., E. Tálas, Z. Pászti, K. Zelenka, I. Ayyubov, K. Salmanzade, I. E. Sajó, G. Sáfrán and A. Tompos. 2021a. Investigation of Ti-Mo mixed oxide-carbon composite supported Pt electrocatalysts: Effect of the type of carbonaceous materials. Applied Catalysis A: General 620: 118155. https://doi.org/10.1016/j.apcata.2021.118155

Borbáth, I., I. Bakos, Z. Pászti, G. P. Szijjártó and A. Tompos. 2021b. Design of SnPt/C cathode electrocatalysts with optimized Sn/Pt surface composition for potential use in Polymer Electrolyte Membrane Fuel Cells. Catalysis Today 366: 20–30. https://doi.org/10.1016/j.cattod.2020.06.029

Cao, X. Q., J. Zhou, S. Li and G. W. Qin. 2020. Ultra-stable metal nano-catalyst synthesis strategy: a perspective. Rare Metals 39(2): 113–130. https://doi.org/10.1007/s12598-019-01350-y

Carrillo-Rodríguez, J. C., I. L. Alonso-Lemus, A. A. Siller-Ceniceros, E. Martínez G, P. Pizá-Ruiz, G. Vargas-Gutiérrez and F. J. Rodríguez-Varela. 2017. Easy synthesis of N-doped graphene by milling exfoliation with electrocatalytic activity towards the Oxygen Reduction Reaction (ORR). International Journal of Hydrogen Energy 42(51): 30383–

30388. https://doi.org/10.1016/j.ijhydene.2017.08.084

Dan, M., A. Vulcu, S. A. Porav, C. Leostean, G. Borodi, O. Cadar and C. Berghian-Grosan. 2021. Eco-Friendly Nitrogen-Doped Graphene Preparation and Design for the Oxygen Reduction Reaction. Molecules 26(3858). https:// doi.org/10.3390/molecules26133858

El-Deen, A. G., M. El-Newehy, C. S. Kim and N. A. M. Barakat. 2015. Nitrogen-doped, FeNi alloy nanoparticle-decorated graphene as an efficient and stable electrode for electrochemical supercapacitors in acid medium. Nanoscale Research Letters 10(1): 1–7. https://doi.org/10.1186/s11671-015-0778-6

Fairley, N. 2006. CasaXPS: Spectrum Processing Software for XPS, AES and SIMS (Version 2.3.13). Retrieved from http://www.casaxps.com/

Gohari-Bajestani, Z., O. Akhlaghi, Y. Yürüm and A. Yürüm. 2017. Synthesis of anatase TiO_2 with exposed (001) facets grown on N-doped reduced graphene oxide for enhanced hydrogen storage. International Journal of Hydrogen Energy 42(9): 6096–6103. https://doi.org/10.1016/j.ijhydene.2016.11.069

González-Hernández, M., E. Antolini and J. Perez. 2020. CO tolerance and stability of PtRu and PtRuMo electrocatalysts supported on N-doped graphene nanoplatelets for polymer electrolyte membrane fuel cells. International Journal of Hydrogen Energy 45(8): 5276–5284. https://doi.org/10.1016/j.ijhydene.2019.05.208

Gopalakrishnan, K., H. M. Joshi, P. Kumar, L. S. Panchakarla and C. N. R. Rao. 2011. Selectivity in the photocatalytic properties of the composites of TiO_2 nanoparticles with B- and N-doped graphenes. Chemical Physics Letters 511(4–6): 304–308. https://doi.org/10.1016/j.cplett.2011.06.033

Hou, R., Y. Jia, F. Wang, D. Huang, X. Lv and H. Wang. 2022. The promoted photocatalytic mechanism of N-doped graphene/TiO_2 composites: From experiment to theory. Diamond and Related Materials 126(May): 109107. https://doi.org/10.1016/j.diamond.2022.109107

Hsieh, B. J., M. C. Tsai, C. J. Pan, W. N. Su, J. Rick, H. L. Chou, J. F. Lee and B. J. Hwang. 2017. Tuning metal support interactions enhances the activity and durability of TiO_2-supported Pt nanocatalysts. Electrochimica Acta 224: 452–459. https://doi.org/10.1016/j.electacta.2016.12.020

Huang, K., K. Sasaki, R. R. Adzic and Y. Xing. 2012. Increasing Pt oxygen reduction reaction activity and durability with a carbon-doped TiO_2 nanocoating catalyst support. Journal of Materials Chemistry 22(33): 16824–16832. https://doi.org/10.1039/c2jm32234j

Huang, S. Y., P. Ganesan and B. N. Popov. 2011. Titania supported platinum catalyst with

high electrocatalytic activity and stability for polymer electrolyte membrane fuel cell. Applied Catalysis B: Environmental 102(1–2): 171–177. https://doi.org/10.1016/j.apcatb.2010.11.026

Hugenschmidt, M. B., L. Gamble and C. T. Campbell. 1994. The interaction of H_2O with a TiO_2(110) surface. Surface Science 302(3): 329–340. https://doi.org/10.1016/0039-6028(94)90837-0

Ida, S., P. Wilson, B. Neppolian, M. Sathish, P. Karthik and P. Ravi. 2019. Ultrasonically aided selective stabilization of pyrrolic type nitrogen by one pot nitrogen doped and hydrothermally reduced Graphene oxide/Titania nanocomposite (N-TiO_2/N-RGO) for H_2 production. Ultrasonics Sonochemistry 57(March): 62–72. https://doi.org/10.1016/j.ultsonch.2019.04.041

Imran Jafri, R., N. Rajalakshmi and S. Ramaprabhu. 2010. Nitrogen doped graphene nanoplatelets as catalyst support for oxygen reduction reaction in proton exchange membrane fuel cell. Journal of Materials Chemistry 20(34): 7114–7117. https://doi.org/10.1039/c0jm00467g

Jiménez-Morales, I., S. Cavaliere, D. Jones and J. Rozière. 2018. Strong metal-support interaction improves activity and stability of Pt electrocatalysts on doped metal oxides. Physical Chemistry Chemical Physics 20(13): 8765–8772. https://doi.org/10.1039/c8cp00176f

Kang, D. Y. and J. H. Moon. 2014. Lithographically defined three-dimensional pore-patterned carbon with nitrogen doping for high-performance ultrathin supercapacitor applications. Scientific Reports 4: 1–8. https://doi.org/10.1038/srep05392

Karabiberoğlu, Ş. U., Ç. C. Koçak and Z. Dursun. 2019. Electrochemical Determination of Dicofol at Nickel Nanowire Modified Poly(p-aminophenol) Film Electrode. Electroanalysis 31(7): 1304–1310. https://doi.org/10.1002/elan.201900095

Lerf, A., A. Buchsteiner, J. Pieper, S. Schöttl, I. Dekany, T. Szabo and H. P. Boehm. 2006. Hydration behavior and dynamics of water molecules in graphite oxide. Journal of Physics and Chemistry of Solids 67(5–6): 1106–1110. https://doi.org/10.1016/j.jpcs.2006.01.031

Li, Y., L. Liu, Y. Wu, T. Wu, H. Wu, Q. Cai, Y. Xu, B. Zeng, C. Yuan and L. Dai. 2019. Facile synthesis of nitrogen-doped carbon materials with hierarchical porous structures for high-performance supercapacitors in both acidic and alkaline electrolytes. Journal of Materials Chemistry A 7(21): 13154–13163. https://doi.org/10.1039/c9ta00890j

Lin, L. Y., Y. Nie, S. Kavadiya, T. Soundappan and P. Biswas. 2017. N-doped reduced

graphene oxide promoted nano TiO_2 as a bifunctional adsorbent/photocatalyst for CO_2 photoreduction: Effect of N species. Chemical Engineering Journal 316: 449–460. https://doi.org/10.1016/j.cej.2017.01.125

Luque-Centeno, J. M., M. V. Martínez-Huerta, D. Sebastián, S. Pérez-Rodríguez and M. J. Lázaro. 2021. Titanium Dioxide/N-Doped Graphene Composites as Non-Noble Bifunctional Oxygen Electrocatalysts. Industrial and Engineering Chemistry Research 60(51): 18817–18830. https://doi.org/10.1021/acs.iecr.1c02896

Majrik, K., Z. Pászti, L. Korecz, L. Trif, A. Domján, G. Bonura, C. Cannilla, F. Frusteri, A. Tompos and E. Tálas. 2018. Study of PtO_x/TiO_2 photocatalysts in the photocatalytic reforming of glycerol: The role of co-catalyst formation. Materials 11(10) 1927. https://doi.org/10.3390/ma11101927

Mastalir, Á., T. Szabó, Z. Király and I. Dékány. 2012. Synthesis and catalytic investigation of organophilic Pd/graphite oxide nanocomposites. Catalysis Communications 17(3): 104–107. https://doi.org/10.1016/j.catcom.2011.10.028

Meier, J. C., C. Galeano, I. Katsounaros, A. A. Topalov, A. Kostka, F. Schu and K. J. J. Mayrhofer. 2012. Degradation Mechanisms of Pt/C Fuel Cell Catalysts under Simulated Start − Stop Conditions. ACS Catalysis 2(5): 832−843. https://doi.org/10.1021/cs300024h

Meier, J. C., C. Galeano, I. Katsounaros, J. Witte, H. J. Bongard, A. A. Topalov, C. Baldizzone, S. Mezzavilla, F. Schüth and K. J. J. Mayrhofer. 2014. Design criteria for stable Pt/C fuel cell catalysts. Beilstein Journal of Nanotechnology 5(1): 44–67. https://doi.org/10.3762/bjnano.5.5

Micoud, F., F. Maillard, A. Gourgaud and M. Chatenet. 2009. Unique CO-tolerance of Pt-WO_x materials. Electrochemistry Communications 11(3): 651–654. https://doi.org/10.1016/j.elecom.2009.01.007

Mohai, M. 2004. XPS MultiQuant: Multimodel XPS quantification software. Surface and Interface Analysis 36(8): 828–832. https://doi.org/10.1002/sia.1775

Mohai, M. 2011. XPS MultiQuant: Multi-model X-ray photoelectron spectroscopy quantification program (Version 7.00.92). Retrieved from http://aki.ttk.mta.hu/XMQpages/XMQhome.php

Mohai, M., K. László and I. Bertóti. 2018. Reduction and covalent modification of graphene-oxide by nitrogen in glow discharge plasma. Surface and Interface Analysis 50(11): 1207–1212. https://doi.org/10.1002/sia.6411

Moulder, J. F., W. F. Stickle, P. E. Sobol and K. D. Bombe. 1992. Handbook of X-ray

Photoelectron Spectroscopy. Minnesota, USA: Perkin-Elmer Corp. Eden Prairie.

Mu, S., X. Chen, R. Sun, X. Liu, H. Wu, D. He and K. Cheng. 2016. Nano-size boron carbide intercalated graphene as high performance catalyst supports and electrodes for PEM fuel cells. Carbon 103: 449–456. https://doi.org/10.1016/j.carbon.2016.03.044

Nagy, B., S. Villar-Rodil, J. M. D. Tascón, I. Bakos and K. László. 2016. Nitrogen doped mesoporous carbon aerogels and implications for electrocatalytic oxygen reduction reactions. Microporous and Mesoporous Materials 230: 135–144. https://doi.org/10.1016/j.micromeso.2016.05.009

Nagy, B., I. Bakos, I. Bertóti, A. Domán, A. Menyhárd, M. Mohai and K. László. 2018. Synergism of nitrogen and reduced graphene in the electrocatalytic behavior of resorcinol - Formaldehyde based carbon aerogels. Carbon 139: 872–879. https://doi.org/10.1016/j.carbon.2018.07.061

Naumkin, A. V., A. Kraut-Vass, S. W. Gaarenstroom and C. J. Powell. 2023. NIST X-ray Photoelectron Spectroscopy Database. https://doi.org/https://dx.doi.org/10.18434/T4T88K

Neaţu, Ş., F. Neaţu, I. M. Chirica, I. Borbáth, E. Tálas, A. Tompos, S. Somacescu, P. Osiceanu, M. A. Folgado, A. M. Chaparro and M. Florea. 2021. Recent progress in electrocatalysts and electrodes for portable fuel cells. Journal of Materials Chemistry A 9(32): 17065–17128. https://doi.org/10.1039/d1ta03644k

Ni, S., F. Han, W. Wang, D. Han, Y. Bao, D. Han, H. Wang and L. Niu. 2018. Innovations upon antioxidant capacity evaluation for cosmetics: A photoelectrochemical sensor exploitation based on N-doped graphene/TiO_2 nanocomposite. Sensors and Actuators B: Chemical 259: 963–971. https://doi.org/10.1016/j.snb.2017.12.154

Özdokur, K. V., Ç. C. Koçak, Ç. Eden, Z. Demir, Ç. Çirak, E. Yavuz and B. Çağlar. 2022. Gold-Nanoparticles-Decorated ZrO_2-CuO Nanocomposites: Synthesis, Characterization and A Novel Platform for Electrocatalytic Formaldehyde Oxidation. ChemistrySelect 7(28) e20220141. https://doi.org/10.1002/slct.202201411

Park, S., Y. Shao, H. Wan, P. C. Rieke, V. V. Viswanathan, S. A. Towne, L. V. Saraf, J. Liu, Y. Lin and Y. Wang. 2011. Design of graphene sheets-supported Pt catalyst layer in PEM fuel cells. Electrochemistry Communications 13(3): 258–261. https://doi.org/10.1016/j.elecom.2010.12.028

Patil, P. O., S. N. Nangare, P. P. Patil, A. G. Patil, D. R. Patil, R. S. Tade, A. M. Patil, P. K. Deshmukh and S. B. Bari. 2021. Fabrication of N-doped Graphene@TiO_2 nanocomposites for its adsorption and absorbing performance with facile recycling.

Nano Biomedicine and Engineering 13(2): 179–190. https://doi.org/10.5101/NBE.V13I2.P179-190

Patterson, A. L. 1939. The Scherrer formula for X-ray particle size determination. Physical Review 56(10): 978–982. https://doi.org/10.1103/PhysRev.56.978

Salgado, J. R. C., F. Alcaide, G. Álvarez, L. Calvillo, M. J. Lázaro and E. Pastor. 2010. Pt-Ru electrocatalysts supported on ordered mesoporous carbon for direct methanol fuel cell. Journal of Power Sources 195(13): 4022–4029. https://doi.org/10.1016/j.jpowsour.2010.01.001

Somacescu, S., P. Osiceanu, J. M. Calderon Moreno, D. C. Culita, F. Neațu, M. M. Trandafir, Ștefan Neațu, A. Kuncser, G. P. Szijjártó, E. Tálas, A. Tompos, I. Borbáth and M. Florea. 2023. Design of electrocatalysts with reduced Pt content supported on mesoporous $NiWO_4$ and $NiWO_4$-graphene nanoplatelets composite for oxygen reduction and hydrogen oxidation in acidic medium. International Journal of Hydrogen Energy 48(16): 6317–6335. https://doi.org/10.1016/j.ijhydene.2022.04.270

Stobinski, L., B. Lesiak, J. Zemek and P. Jiricek. 2012. Time dependent thermal treatment of oxidized MWCNTs studied by the electron and mass spectroscopy methods. Applied Surface Science 258(20): 7912–7917. https://doi.org/10.1016/j.apsusc.2012.04.127

Sundriyal, S., M. Sharma, A. Kaur, S. Mishra and A. Deep. 2018. Improved electrochemical performance of rGO/TiO_2 nanosheet composite based electrode for supercapacitor applications. Journal of Materials Science: Materials in Electronics 29(15): 12754–12764. https://doi.org/10.1007/s10854-018-9393-5

Takabatake, Y., Z. Noda, S. M. Lyth, A. Hayashi and K. Sasaki. 2014. Cycle durability of metal oxide supports for PEFC electrocatalysts. International Journal of Hydrogen Energy 39(10): 5074–5082. https://doi.org/10.1016/j.ijhydene.2014.01.094

Thakur, A. K., R. B. Choudhary, M. Majumder and M. Majhi. 2018. Fairly improved pseudocapacitance of PTP/PANI/TiO_2 nanohybrid composite electrode material for supercapacitor applications. Ionics 24(1): 257–268. https://doi.org/10.1007/s11581-017-2183-x

Vass, Á., I. Borbáth, Z. Pászti, I. Bakos, I. E. Sajó, P. Németh and A. Tompos. 2017. Effect of Mo incorporation on the electrocatalytic performance of Ti–Mo mixed oxide–carbon composite supported Pt electrocatalysts. Reaction Kinetics, Mechanisms and Catalysis 121(1): 141–160. https://doi.org/10.1007/s11144-017-1155-5

Vass, Á., I. Borbáth, I. Bakos, Z. Pászti, I. E. Sajó and A. Tompos. 2018. Novel Pt Electrocatalysts: Multifunctional Composite Supports for Enhanced Corrosion

Resistance and Improved CO Tolerance. Topics in Catalysis 61: 1300–1312. https://doi.org/10.1007/s11244-018-0988-0

Vass, Á., I. Borbáth, I. Bakos, Z. Pászti, G. Sáfrán and A. Tompos. 2019. Stability issues of CO tolerant Pt-based electrocatalysts for polymer electrolyte membrane fuel cells: comparison of $Pt/Ti_{0.8}Mo_{0.2}O_2$–C with PtRu/C. Reaction Kinetics, Mechanisms and Catalysis 126(2): 679–699. https://doi.org/10.1007/s11144-018-1512-z

Wagner, C. D., A. V. Naumkin, A. Kraut-Vass, S. W. Gaarenstroom, J. C. Powell, W. Allison, C. J. Powell and J. R. J. Rumble. 2003. NIST X-ray Photoelectron Spectroscopy Database. Retrieved June 2, 2021, from https://srdata.nist.gov/xps/

Wang, D., C. V. Subban, H. Wang, E. Rus, F. J. Disalvo and H. D. Abruña. 2010. Highly stable and CO-tolerant $Pt/Ti_{0.7}W_{0.3}O_2$ Electrocatalyst for proton-exchange membrane fuel cells. Journal of the American Chemical Society 132(30): 10218–10220. https://doi.org/10.1021/ja102931d

Wang, H., T. Maiyalagan and X. Wang. 2012. Review on recent progress in nitrogen-doped graphene: Synthesis, characterization, and its potential applications. ACS Catalysis 2(5): 781–794. https://doi.org/10.1021/cs200652y

Wong, W. Y., W. R. W. Daud, A. B. Mohamad, A. A. H. Kadhum, K. S. Loh and E. H. Majlan. 2013. Recent progress in nitrogen-doped carbon and its composites as electrocatalysts for fuel cell applications. International Journal of Hydrogen Energy 38(22): 9370–9386. https://doi.org/10.1016/j.ijhydene.2012.12.095

Xing, T., J. Sunarso, W. Yang, Y. Yin, A. M. Glushenkov, L. H. Li, P. C. Howlett and Y. Chen. 2013. Ball milling: A green mechanochemical approach for synthesis of nitrogen doped carbon nanoparticles. Nanoscale, 5(17): 7970–7976. https://doi.org/10.1039/c3nr02328a

Yamada, Y., H. Yasuda, K. Murota, M. Nakamura, T. Sodesawa and S. Sato. 2013. Analysis of heat-treated graphite oxide by X-ray photoelectron spectroscopy. Journal of Materials Science 48(23): 8171–8198. https://doi.org/10.1007/s10853-013-7630-0

Yan, W. Y., Q. Zhou, X. Chen, X. J. Huang and Y. C. Wu. 2016. C-doped and N-doped reduced graphene oxide/TiO_2 composites with exposed (0 0 1) and (1 0 1) facets controllably synthesized by a hydrothermal route and their gas sensing characteristics. Sensors and Actuators B: Chemical, 230: 761–772. https://doi.org/10.1016/j.snb.2016.02.133

Yazici, M. S., S. Dursun, I. Borbáth and A. Tompos. 2021. Reformate gas composition and pressure effect on CO tolerant $Pt/Ti_{0.8}Mo_{0.2}O_2$–C electrocatalyst for PEM fuel cells.

International Journal of Hydrogen Energy 46(25): 13524–13533. https://doi.org/10.1016/j.ijhydene.2020.08.226

Yun, Y. S., D. Kim, Y. Tak and H. J. Jin. 2011. Porous graphene/carbon nanotube composite cathode for proton exchange membrane fuel cell. Synthetic Metals 161(21–22): 2460–2465. https://doi.org/10.1016/j.synthmet.2011.09.030

Zana, A., C. Rüdiger, J. Kunze-Liebhäuser, G. Granozzi, N. E. A. Reeler, T. Vosch, J. J. K. Kirkensgaard and M. Arenz. 2014. Core-shell TiO_2@C: Towards alternative supports as replacement for high surface area carbon for PEMFC catalysts. Electrochimica Acta 139: 21–28. https://doi.org/10.1016/j.electacta.2014.07.002

Zhang, N., M. Q. Yang, S. Liu, Y. Sun and Y. J. Xu. 2015. Waltzing with the Versatile Platform of Graphene to Synthesize Composite Photocatalysts. Chemical Reviews 115(18): 10307–10377. https://doi.org/10.1021/acs.chemrev.5b00267

Zhang, Z., J. Liu, J. Gu, L. Su and L. Cheng. 2014. An overview of metal oxide materials as electrocatalysts and supports for polymer electrolyte fuel cells. Energy and Environmental Science 7(8): 2535–2558. https://doi.org/10.1039/c3ee43886d

Zhao, J., Z. Tu and S. H. Chan. 2021. Carbon corrosion mechanism and mitigation strategies in a proton exchange membrane fuel cell (PEMFC): A review. Journal of Power Sources 488: 229434. https://doi.org/10.1016/j.jpowsour.2020.229434

Zhao, Y., G. Wang, L. Li, X. Dong and X. Zhang. 2020. Enhanced activation of peroxymonosulfate by nitrogen-doped graphene/TiO_2 under photo-assistance for organic pollutants degradation: Insight into N doping mechanism. Chemosphere 244: 125526. https://doi.org/10.1016/j.chemosphere.2019.125526

Zheng, P., W. Zhou, Y. Wang, D. Ren, J. Zhao and S. Guo. 2020. N-doped graphene-wrapped TiO_2 nanotubes with stable surface Ti^{3+} for visible-light photocatalysis. Applied Surface Science 512: 144549. https://doi.org/10.1016/j.apsusc.2019.144549